Mehran University Research Journal of Engineering and Technology

https://doi.org/10.22581/muet1982.2401.2873

2024, 43(1) 129-141

Fabrication of low-cost and environmental-friendly EHD printable thin film nanocomposite triboelectric nanogenerator using household recyclable materials

Muzamil Hussain Memon [a], Maria Mustafa [a, *], Zeeshan Ali Abro [b]

[a] *Department of Chemical Engineering, COMSATS University Islamabad Lahore Campus, Punjab 54000 Pakistan*

[b] *Department of Environmental Engineering, USPCAS-W Mehran University of Engineering and Technology, Jamshoro Sindh 76062 Pakistan*

[*] Corresponding author: Maria Mustafa, Email: mariamustafa@cuilahore.edu.pk

Received: 13 June 2023, Accepted: 20 December 2023, Published: 01 January 2024

K E Y W O R D S

Electronic Waste

Carbon Dots CDs

Energy Harvester

EHD Printable

Fabrication

TENG

A B S T R A C T

Humans generate massive amounts of plastic and electronic waste, which pollute our environment, particularly our water supplies, and cause fatal difficulties. In addition, the increased use of fossil fuels is wreaking havoc on the ecosystem. In order to solve these issues, we describe a simple, low-cost, and environmentally-friendly triboelectric nanogenerator (TENG) made of electronic waste and recycled plastic, and we add nanomaterial to improve power generation using biomechanical energy. The present investigation involves synthesizing carbon dots (CDs) nano-material through a single-step hydrothermal technique and CDs nano-material characterized via UV.Vis Spectroscopy. The proposed carbon dot-graphite nano composite-based TENGs (CGC-TENGs) are created by reusing dry cells (electronic waste) to obtain graphite, plastic bottles to obtain plastic, and synthesized CDs. CGC-TENGs manufactures a simple, low-cost, and environmentally friendly In-house quick and bulk fabrication printed electro hydrodynamics (EHD) electrospray process that uses less solvent and does not require specialist equipment or knowledge. Comparing fabricate TENG device results, in which CDs used produced high voltage (127.31 V)/current (107.12 μA), while not using CDs produced low voltage (95.23 V)/current (104.12 μA) at similar fabrication parameters, the size of the devices are 4.5 cm × 7 cm, and 15 N force applied. The CGC-TENG (δ) has maximum output performance and is thoroughly investigated using an open-circuit voltage of 171.30 V, a short circuit current of 111.39 μA, and a maximum output power density of 53.08 μW/cm^2. CGC-TENG (δ) was used to power an electronic glucose monitoring device, and twenty-three blue light-emitting diodes (LEDs) to demonstrate its practical applications. The approach we propose produces renewable energy sources by reutilizing plastic waste and technological waste, providing a practical and sustainable path toward our goal of creating a green planet.

1. Introduction

In the last few decades of technological breakthroughs, the modern world has been fast changing, resulting in a massive increase in electric gadgets, for example, digital cameras, cell phones, computers, and different IoT devices [1-3]. According to recent research by the International Renewable Energy Agency (IREA), it is estimated that by the end of 2025, over 70 billion electronic devices will be connected to the Internet, surpassing 35.8 billion devices [4]. The increased use of electronic devices generates severe environmental issues by producing electronic waste. According to estimates, global electronic waste creation is expected to exceed 111 million tonnes by 2050. Because bulk electronic gadgets are battery-driven, worldwide battery demand is growing and is expected to spread around (70 GWh) by the end of 2035 [5-7]. Such as a result, a substantial fraction of electronic waste is abandoned batteries, particularly non-rechargeable batteries [8, 9].

Furthermore, most of these batteries include harmful compounds such as carbon metals, which are slowly discharged into the surroundings and represent substantial hazards to human health and the surroundings. When harmful items are discarded in landfills, they can leach into the soil and enter our water supply. Poisonous gases are released when burnt, endangering the environment and human health [10, 11]. Metal-carbon batteries and polymers have some environmental and health effects. As a result of these implications, numerous recycling methods for battery materials have been developed. However, the described techniques have mainly concentrated on recycling the battery's metal component while overlooking the reutilizing of the battery's carbon-based component [12-16].

Plastic trash contributes to ecological issues like air pollution, soil contamination, water pollution, rising temperatures, and so on [17,18]. For example, the "Great Pacific Garbage Patch" covers 1.5×10^{-3} $MMkm^2$ of the Pacific Ocean, with most garbage being plastic waste [19, 20]. According to projections, worldwide plastic trash will reach over 12000 million tonnes by 2060 [21, 22]. Plastic bottles hold food and drink, the most common source of domestic waste, as most of these flasks are never reused. The increased use of plastic bottles is driving manufacturing and is estimated to exceed by the end of this year 585 billion units. As a result, it is critical to reuse bottles and use them resourcefully and sustainably [23, 24].

Energy has historically been a vital component of human life. We have numerous energy sources around us, including heat, wind, and light, where mechanical energy sources lead significantly, as low-frequency mechanical vibrations are commonly detected. TENGs have emerged as a low-cost, effective, and efficient energy source for less power consumption portable sensors and electronic gadgets like torches, calculators, LEDs, smart bracelets, and pH sensors [25-28]. TENGs are a potential technology because they can generate electrical output using electrostatic induction and triboelectric charging principles from various low frequencies, environmental, and mechanically driven sources. TENG's manufacturing is also low-cost or scalable, making it preferable to supplementary a low-frequency energy source. TENGs have traditionally been manufactured using expensive components and complex fabrication techniques such as triboelectric material modification and liquid metal [29-33].

Several methods for producing TENGs from waste materials have been proposed; one early study gathered supermarket bags, poly bags, and sponges via trash to create triboelectric layers, and electrodes were created with aluminum foil. Another study made the triboelectric layer out of rubber tires and used aluminum foil as an electrode. The use of heat glasses reactors and spin-dip coating processes complicates fabrication. Broken tea leaves were also recycled as a recovered triboelectric layer, and aluminum was removed from used aluminum waste plastic bags. A compaction was employed to press the aluminum sheet and the broken tea leaves [34-37].

Furthermore, mixing strain gauges plus TENG was developed by reusing plastic-based bags. The combination of a strain detector and a TENG complicates the overall structure. Only the substrate was reused from waste plastic bottles in the following study. In addition, plastics use a negatively charged triboelectric layer. Then, triboelectric layers were created using recycled plastic bags, and gold-based electrodes were created via vacuum deposition sputtering. The use of gold-based electrodes increases the cost of the manufacturing process. Face-masks were repurposed, and electrodes were developed using sticky copper (tape). Disinfection of facial masks increases the manufacturing time and cost [38-41].

CDs are nanoparticles with quasi-spherical shapes and sizes less than 10nm. CDs were discovered in 2004 as a new family member of the nano-carbon. Apart from being environmentally friendly. It is also potential in

nanoelectronics and also in biomedical applications due to less harmful material. The CD's toxicity measurement depends on various factors, i.e., concentration, size, surface chemistry, etc. However, the exact reason is still unknown due to insufficient scientific research. The CDs have a variety of benefits, including conductivity, biocompatibility, light bleaching properties, high solubility, and so on [42-45]. CDs have exceptional photoluminescence properties, which explains their efficacy in fluorescence labeling, chemical sensing, light-emitting diodes, and biological sensing. CDs can be used as a shell material. A formless or sp2-sp3 hybrid crystal emerges from the central carbon core. Defects, as well as functional groups on the surface such as carbonyl (C- -O), amino (-NH2), hydroxyl (-OH), carboxyl (-COOH), epoxy (-CH(O)CH-), sulfonic (-HSO3), and cyano, are present in the spherical shell. (-CN). CDs containing these functional compounds disperse well in solvents and interact actively with various materials [46, 47].

Electrohydrodynamic (EHD) inkjet printing is a non-contact, additive, and direct-writing technology that has benefits in prototype and large-level manufacturing due to its cost-effective efficacy, low waste, and quick output. EHD printable electrospray methods deposit thin films with high control and precision. They have several benefits versus spinning depositing, such as more excellent resolution, fine layer control, adaptability, trim waste, and quick fabrication. These methods may deposit various materials and are appropriate for various applications such as sensors, electronics, and even biomedicine. In this process, an electric field is applied between a printing nozzle and a target substrate to emit the microscale droplets and print the microscale functional patterns. EHD inkjet printing can create microscale grid patterns that are invisible to the naked eye [48-51]. The grid structure of carbon-based printed electrodes also ensures mechanical robustness and adaptability. As a result, wearable and flexible TENGs have been created using carbon-based EHD-printed electrodes [52].

To reduce pollution and produce valuable eco-friendly energy, we developed a low-cost and environmentally friendly triboelectric nanogenerator (TENG) by recycling e-waste (dry cells) to obtain graphite and unwanted plastic for triboelectric materials. For the preparation of conductive ink, recovered graphite is blended with CDs for EHD printable TENGs, where CDs improve the performance of the TENGs. Using these waste products aids in reducing waste in the environment and promotes the circular economy. The suggested CGC-TENG is made quickly in the home without using expensive equipment, environment, or experience. The three prototype devices performed admirably, but the highest performance is CGC-TENG (δ), obtaining a voltage of 171.30 (V), a short-circuit current of 111.39 (μA), and a maximum electrical output of power density of 53.08 ($\mu W/cm^2$). The CGC-TENG powers an electronic glucose monitoring device and twenty-three blue LEDs to show its practical applications in portable, less-power-effective electronic devices. CGC-TENG reduces environmental pollutants while also producing energy, promoting the long-term growth of self-powered portable devices.

2. Material and Methodology

2.1 Materials, Synthesis of Carbon Dots (CDs), and Characterization

For the synthesis of carbon dots, all raw materials were bought analytical grade from Sigma-Aldrich, i.e., Ascorbic Acid (A92902), Ethylenediamine (E26266, ≥99% pure), and Acetone (270725, ≥99% pure). The CDs were prepared using a single-step hydrothermal technique. In 50 mL deionized water, 1 g ascorbic acid and 1 mL ethylenediamine were dissolved using a magnetic stirrer for 20 min at 1000 rpm, and further, the solution was sonicated for 15 min. The solution was placed in a stain steel autoclave lined with Teflon and heated at 200 °C for 8 hrs. After heating, the autoclave was cooled to room temperature, and the resulting CDs solutions were centrifuged at 4500 rpm for 20 min. After that, the solutions were filtered through a microporous membrane with a pore size of 0.22 μm, precipitated wash with acetone, and dried in a hot air dryer at 90 °C for 18 hrs; after cooling at room temperature, the material was stored in a moisture and dust-free container until testing. Fig. 1 depicts the complete technique for synthesizing CDs using Ascorbic Acid with the hydrothermal method. UV-Spectroscopy model is Biotechnology Medical Services (BMS)/ UV 1602 characterized the Carbon Dots synthesized material.

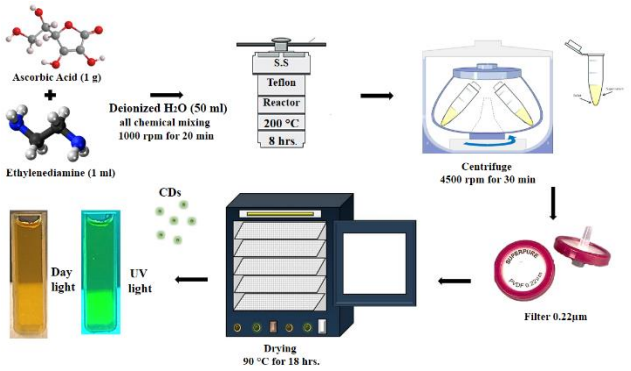

Fig. 1. Synthesis CDs using Single Step Hydrothermal Method Process flow

2.2 Printable CDC-TENG Device Fabrication

2.2.1 Materials

CGC-TENG was primarily made of recyclable materials. The plastic utilized in the device's construction was cut from smooth surfaces of water bottles and plastics gathered from a house rubbish bin. Before usage, the reusable plastic was thoroughly washed with deionized water and dried at 20 ºC. Graphite was recovered from dry cells obtained from the local market. The gel-ink from a local market present gel-pen (Dollar Gel-1' Black-Pen) was combined with the Carbon Dots CDs and the Graphite composite (CGC) material for the preparation of conductive ink paste for the fabrication of CGC-TENG's active layer and the use of Copper (Cu) and Aluminum (Al) tape as an electrode. As a flexible substrate material for triboelectric or active layers and electrodes, chart paper (0.25 mm thickness) was used. Copper wires were utilized to connect the electrodes of the CGC-TENG to the external circuitry and operate portable electronic devices like the electronic glucose monitoring device, which required 9.6 µW of power, respectively.

2.2.2 Preparation of carbon dots graphite composite (CGC) conductive ink for thin film formation

The graphite material retrieved from a dry cell produced composite conductive ink. After removing the graphite electrode from the used dry cell, rinsing it twice with de-ionized water, and then cleaning it with cotton fabric, the graphite electrode is pulverized (micronized) manually with a porcelain mortar and pestle. In the end, the polarised graphite powder and the carbon dots powder were mixed to make a composite material known as CGC powder with a ratio of 1:0.25. This powder was then utilized as a conductive paste. The weight of graphite and carbon dots and the volume of gel pen ink were measured with the help of a lab analytical digital electronic weight balance (Joanlab RS-232) and a measuring porcelain crucible cup, respectively. After combining gel pen ink with CGC powder as a binder and dissolving the mixture in 1 ml of acetone per 5 ml of solution (CGC solution), the conductive ink is sonicated for 40 min at 25 ºC before developing a thin film.

2.2.3 Preparation of thin films for printable CGC-TENG device

To create a thin film (active layer), the prepared conductive ink (CGC solution) is poured into a 5 ml syringe, and then the syringe is attached to a printable EHD-based electrospray system, as depicted in Fig. 2(a). The following components are included in a printable spray setup: a syringe, a nozzle made of stainless steel, a pump, a supply of direct current voltage, a microscope lens, a laptop, and a stage for substrates. Three sizes of CGC-TENG (α, β, and δ) devices are fabricated; dimensions are 2.5 cm x 7 cm, 4.5 cm x 7 cm, and 6.5 cm x 7 cm, respectively. Operating parameters for thin film forming printing machines include spray nozzle 28-gauge size (ID = 184 micrometers and OD = 350 micrometers), flow rate of 0.33 gtt/min for 5hrs, and direct current D.C voltage of 1.5 K.V. The thin film (active layer) was then created on the chart paper using conductive paste and an electrospray setup on the above sizes. The resistances of thin films made with mere ink of gel-pen and with CGC powder conductive paste added are plotted. After the thin film was created, the paper-based substrate was dried out at normal temperature in an ambient condition.

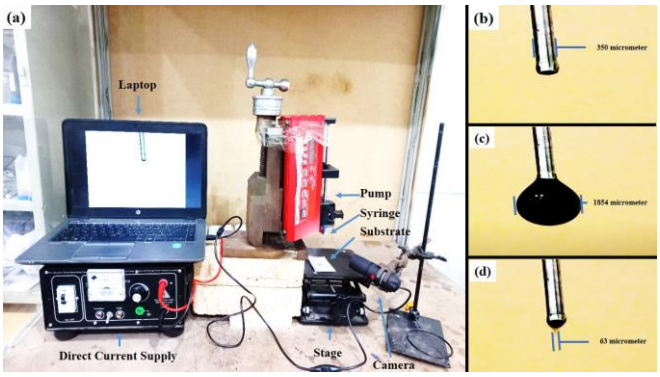

Fig. 2. (a) Printable Thin Film Setup (b) EHD No Droplet Formation (c) EHD Droplet Formation (d) EHD Taylor Jet Cone Formation

2.2.4 CGC-TENG device assembling

To fabricate the various sizes of the CGC-TENG device (α, β, and δ), the length and width are 2.5 cm x 7 cm, 4.5 cm x 7 cm, and 6.5 cm x 7 cm, respectively. These are divided into two sections, with the upper portion forming the CGC/paper/plastic thin film as the active layer and aluminum as an electrode. The lower portion forms the CGC/paper thin layer as the active layer and

copper as the electrode, with a 2 cm sponge (Molty foam) used as a separating material, as shown in Fig. 3.

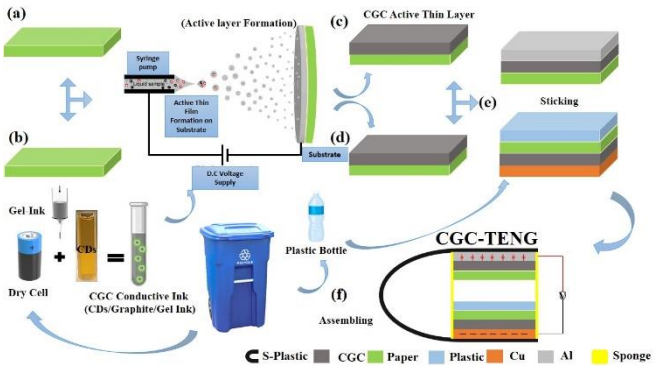

Fig. 3. Illustrations of the CGC-TENG production process in schematic form: Both (a) and (b) include using paper as a substrate for producing active thin films. In (c, and d), the conductive paste is electrospray onto the paper substrate using printable EHD technology. (e) A sheet of plastic salvaged from a used plastic bottle is adhered to the back of an active layer using double-sided tape. Assembly of a triboelectric pair (f) concludes the manufacturing procedure.

2.3 Investigation of CDC-TENG Device

The resistances of the triboelectric layers and electrodes were examined using a Uni-T digital multimeter (UT33B). The electricity-producing performance of the CGC-TENGs was evaluated when a mechanical tapping device supplied external mechanical energy. A virtual digital-oscilloscope (NI VB-8012) was used to examine the electric signals generated via CGC-TENGs continuously.

3. Result and Discussion

3.*1 Characterize Carbon Dots using UV- Spectroscopy*

It was observed that when the synthesized CDs sample was put in the UV light, the color of the CDs sample transformed from a hue that was brilliant yellow when seen with visible light to a hue that was sea green when seen with UV light. This transformation is depicted in Fig. 4. According to the results of the UV-Vis investigation, the CDs sample exhibits absorption bands; the peak that can be seen at 264 nm is attributed to the (n- π*) transitions of (C=O) bonds, while the shoulder that can be seen at 301 nm is attributed to the (π-π *) transitions of aromatic (C=C) bonds. These transitions can be seen in the spectrum [53, 54]. When CDs sample was analysed in the UV-Vis, the concentrated sample of 0.5 ml was diluted in 20 ml of deionized water before it was analyzed.

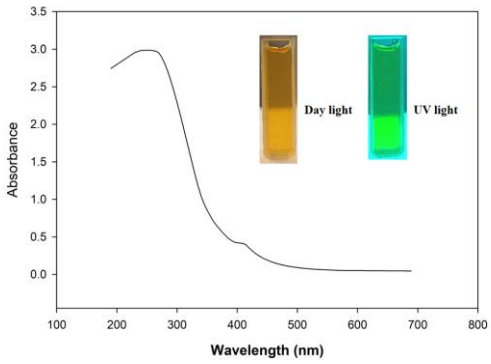

Fig. 4. CDs UV-Vis Analysis Results

3.2 CGC-TENGs Fabrication

The motivation for developing the CGC-TENGs is to utilize waste materials and construct them simply without using expensive specialized equipment. It has been noticed that Fig. 2 (b, c, and d) demonstrates that the droplet and the Taylor jet cone formation take place when variations in voltage and current. The voltage supply and flow-rate parameters of the EHD-printed electrospray setup for thin film creation as an application of fabricating triboelectric nanogenerator TENGs are shown in Fig. 2 (a). It is observed that the voltage and flow rate are not applied, nor a droplet nor a Taylor jet cone is formed (see Fig. 2b). The droplet 1854 mm creation is seen in Fig. 2 (c), but there is no Taylor jet cone formed in the region where the flow rate was applied, but no voltage was given. Fig. 2(c) demonstrates that the Taylor jet cone formation has a droplet size of 63 mm when the applied voltage is 1.5 K.V, and the flow rate is 0.33 gtt/hr. These droplet size analyses were performed with the "Imagej" software. The software allowed us to add the electrospray nozzle size outside diameter, OD = 350 micrometers, and then interpret available data.

Fig. 5 (a-e) displays the findings of the optical microscope (B series: SC1603-CK) at 200x active thin film layer production before and after on the paper substrate and other supporting components such as aluminum, copper, and plastic. This was done on the paper substrate. The magnified results of the material surface pictures demonstrate that the surface is rough and uneven and observe the quality of the material used to fabricate CGC-TENGs. The process by which the paper fiber absorbed the conductive ink and altered the surface of the paper substrate is depicted in detail in Fig. 5 (a and b).

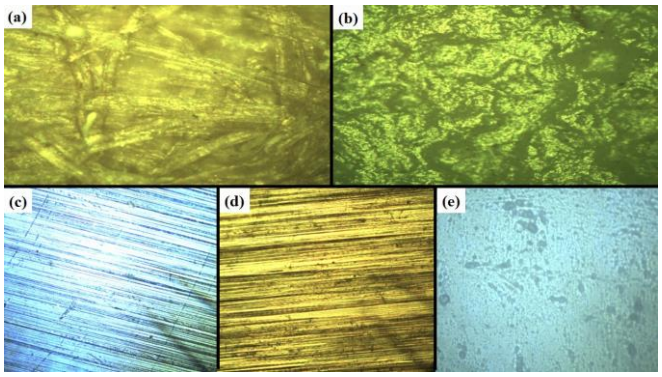

Fig. 5. The findings of a 200x optical microscopy (a) paper substrate before the active thin film layer development, (b) After the formation of the active thin film layer on the paper-based substrate, (c) Aluminum (Al) substrate, (d) Copper (Cu) substrate. (e) Plastic substrate

3.3 CGC-TENGs' Fundamental Working Mechanism

The CGC-TENG employs triboelectric materials with opposing polarities, such as plastic substrate and paper. Fig. 6 depicts the precise working mechanism or principle of CGC-TENG in vertical contact and separation function mode, which is based on the electrostatic induction and the electrification of contact coupling impact. The manufactured CGC-TENG generates significant voltage and current from mechanical energy that is continuously imparted. The synergistic impact of the CGC-TENG active layer dipoles, namely electroactive graphite and carbon dots (CDs), may explain how CGC-TENG works. Strong electrostatic relationships between CDs molecules and the negative dipoles of the CGC-TENG matrix result in the construction of electroactive graphite during the formation of hydrogen bonds when CD particles are present in the complex matrix. While a periodic applied mechanical or biomechanical force is to the CGC-TENG, a secondary-potential is created in the CDs molecules, which arranges the CGC dipoles in the way that follows the mechanical or biomechanical force is applied, which encourages stress-associated polarisation. Vertical contact compression of the CGC-TENG produces a positive potential at the upper part of the aluminum (Al) electrode and a negative potential at the lower part of the copper (Cu) electrode due to self-polarization caused by deformations of the crystalline framework of the CDs-doped graphite nanocomposite and various triboelectric materials. (CGC active layer). In conjunction with self-polarization, the potential difference between the two electrodes regulates electron flow from one electrode to another via an external load. The triboelectric potential decreases immediately when the compressive force is abruptly released. Electrons grouped at the lower part of the electrode are returned to the additional electrode through the external circuit, resulting in an electrical output (voltage and current) with the polar opposite polarity. This process is repetitive in the CGC-TENG under continual compression and relaxation to obtain the electrical performance output (voltage and current) signals from the triboelectric nanogenerator energy harvester gadgets [55-58]. Furthermore, Maxwell's equations can demonstrate the CGC-TENG device's operation. Because of local invariance, Maxwell's equations stay constant in electrodynamics, which can be signified in the following equation.

$$\nabla . J + \frac{d}{dt} \times (\nabla . D) = 0 \quad (1)$$

$$\frac{dp}{dt} + (\nabla . J) = 0 \quad (2)$$

This is known as the continuity equation. Where (p) and (J) are the overall charge density and current density, respectively.

The charge density is expressed as

$$p = pi + pb \quad (3)$$

Where (Jf) denotes free costs, and (Jb) denotes bound charges.

The current density is denoted by

$$J = Jf + Jb \quad (4)$$

Where (Jf) denotes free currents, and (Jb) denotes bound currents.

Auxiliary fields, which play an active role in dipole production in dielectric materials, can be characterized as

$$D \times (\mathrm{r}, \mathrm{t}) = e0 \times E \times (r, t) + P \times (r, t) \quad (5)$$

$$\mathrm{H} \times (r, t) = \frac{B \times (r,t)}{uo} - M \times (r, t) \quad (6)$$

There (D) stands for displacement field; (e0) stands for free space permittivity; (E) stands for the electric field; (P) stands for polarisation; (H) stands for the magnetic field; (uo) stands for free space permeability; (B) stands for magnetic induction; (M) stands for magnetization.

Maxwell's equations could be used to define the operating mechanism of our current work technology. Free charges and current will be used to solve Maxwell's equations.

$$\nabla \mathrm{xH} = \mathrm{Jf} + \frac{\mathrm{dD}}{\mathrm{dt}} (\text{Ampee's circuital law with correction}) \quad (7)$$

$$\nabla \times \mathrm{D} = \mathrm{Pf} \ (\text{Guss's law of electrostatics}) \quad (8)$$

$$\nabla \mathrm{xE} = -\frac{\mathrm{dB}}{\mathrm{dt}} \ (\text{Faraday's law}) \quad (9)$$

$$\nabla \times \mathrm{H} = 0 \ (\text{Magnetostatics of Gauss's law}) \quad (10)$$

The electric field is represented by (E), the displacement electric field by (D), magnetic induction by (B), the magnetic field by (H), the free electron volume charge density by (Jf), and the current density due to free electron flow by (Pf).

Electrodynamics can calculate the displacement current for an electric field and the polarisation current for an electric polarization.

$$J = e0\frac{dE}{dt} \tag{11}$$

$$\mathrm{Jp} = \frac{\mathrm{dP}}{\mathrm{dt}} \tag{12}$$

Thus, the overall displacement current (JD) in a linear isotropic medium is represented by the 2nd term of Maxwell's 4th equation. (Eq. 7).

$$\mathrm{JD} = \frac{\mathrm{dD}}{\mathrm{dt}} = e0\frac{\mathrm{dE}}{\mathrm{dt}} + \frac{\mathrm{dP}}{\mathrm{dt}} \tag{13}$$

Total displacement current is a time-dependent quantity affected by the dielectric medium's electric field and polarization. The first term of Eq. (13) improves the output efficiency of wireless systems such as radio, Wi-Fi, etc. In contrast, the second term improves the piezoelectric effect by increasing (P), which is determined by the applied force or strain.

$$\mathrm{Pi} = (\mathrm{e})\mathrm{ijk} \times (\mathrm{S})\mathrm{jk} \tag{14}$$

$$\mathrm{T} = \mathrm{CeS} - e^{T}\mathrm{E} \tag{15}$$

$$\mathrm{D} = eS - kE \tag{16}$$

Where (S) is the mechanical strain, (e)ijk is the piezoelectric third-order tensor, (T) is the stress tensor, (Ce) is the elasticity tensor, and (k) is the dielectric tensor. A linear polarising medium's displacement current is

$$J_{Di} = \frac{\mathrm{dPi}}{\mathrm{dt}} \tag{17}$$

As a result of Eq. (17), the piezoelectric effect and output current density are proportional to the rate of change of applied force or strain. As a result, achieving the output value of CGC-TENG by applying force corresponds to the theoretical equations.

When there is no external field (E) on a dielectric medium, displacement current depends simply on polarization (from Eq. (17)). Taking the polarization along the z-axis (α), we may write.

$$\mathrm{D}\alpha = \mathrm{P}\alpha = 6P(\alpha) \tag{18}$$

Where $6P(z)$ is the material's piezoelectric polarisation surface charge density. The displaced current term along the z direction (α) will then be calculated.

$$J_{D\alpha} = \frac{\mathrm{dP}\alpha}{\mathrm{dt}} = \frac{\mathrm{d6p}(\alpha)}{\mathrm{dt}} \tag{19}$$

The preceding equation clearly shows why the CGC-TENG gadget has a high output performance.

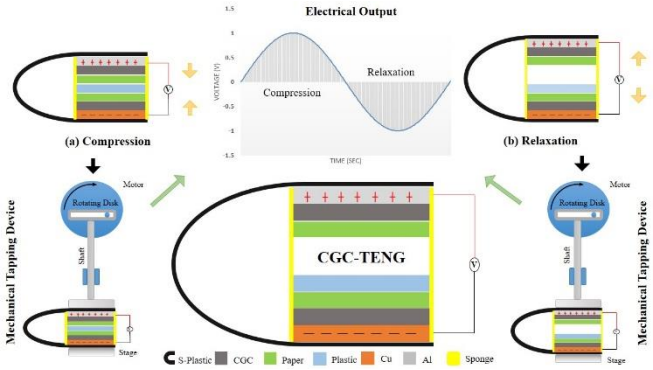

Fig. 6. The Working Principle of CGC-TENGs is illustrated schematically.

3.4 Study of CGC-TENGs Performance

With the assistance of CDs/graphite active layer and plastic, we constructed a TENG energy harvesting device called CGC-TENG for this work. To assess the performance of the CGC-TENGs (α, β, and δ), various electrical output analysis characteristics are plotted and recorded on the output voltage graphs versus time presented in Fig. 7(a). The electrical output voltage (V) and current (μA) are produced by continuous mechanical tapping that imparts and releases a constant axial pressure of 15 N with 7 Hz. This process is repeated indefinitely. Fig. 7(b) illustrates the characteristic of the constructed CGC-TENGs (α, β, and δ) known as the current versus time output Fig. 7(b).

During mechanical tapping impartation, the electrical output (voltage (V) and current (μA)) performance of the CGC-TENGs is at a high level. CGC-TENGs (α, β, and δ) output voltages are 92.61 V, 127.31 V, and 171.30 V. The short circuit currents are 78.76 μA, 107.12 μA, and 111.39 μA, respectively; both voltage (V) and current (μA) are measured by a virtual digital oscilloscope (NI VB-8012) (see Fig. 7(a) and (b)). The inconsistency of the provided strain on the TENG energy harvester flexibility and responsiveness device during mechanical tapping impartation is primarily to blame for the modest variation in the peak values of the output voltage (V) and current (μA) that occurs through rare releasing and pressing. Positive peaks can be seen in the data when the device is subjected to strain, whereas negative peaks can be seen when the device is allowed to recover from the strain and return to its original form. As a result of the dampening effect that the device has, further tiny peaks have been obtained.

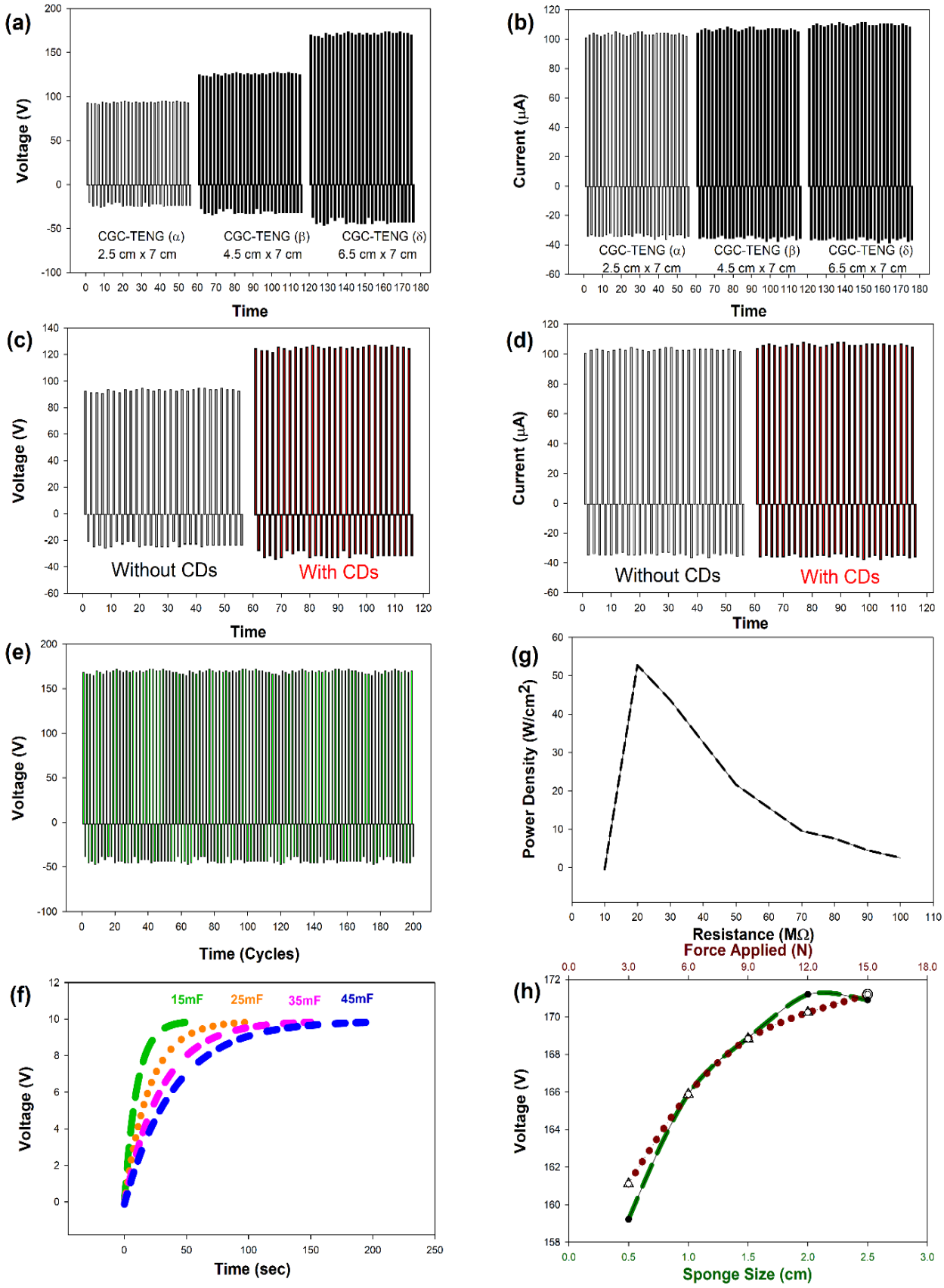

Fig. 7. CGC-TENGs device generates electricity characteristics (α, β, and δ): (a and b) Operating output voltage (V)/current (μA) of a device of increasing size. (c and d) A comparison of the output voltage (V)/current (μA) during the manufacture with and without using CDs. (e) An evaluation of the CGC-TENG output voltage at the various intervals of manufacture and later 20000 cycles or rounds. (f) Time-dependent charging curves for various capacitors. The rectified voltage from the full-bridge rectifier is stored in the capacitors. (g) Power density vs Resistance graph. (h) Effect of sponge size and force applied on voltage generation using CGC-TENG.

A comparison of the impact of Carbon Dots CDs on a triboelectric nanogenerator device's electrical output performance (voltage and current) can be shown in Fig. 7 (c and d). In a triboelectric nanogenerator device, the findings show a voltage (127.31 V) and a current (107.12 µA) obtained when CDs were used; in contrast, the results of not using CDs also show a voltage (95.23 V) and a current (104.12 µA) were acquired. This is evidenced by the fact that the electrical output (voltage (V) and current (µA)) performance of CGC-TENG, which is 1.34 % V and 1.03 % µA with CDs present, is significantly higher than the output performance of CGC-TENG without CDs present when both devices same applied force 15 N.

Fig. 7 (e) depicts the voltage output evaluation of the as-formed CGC-TENG later 20000 cycles or rounds to examine its long-lasting durability. These charts show no noticeable decline in voltage, showing that the CGC-TENG has solid mechanical durability and stability and can power portable electronic devices reliably over a lengthy period. Another vital parameter to consider when evaluating the performance of a nanogenerator is power density. As a result, multiple load resistances have been used to optimize the electrical power density of CGC-TENG, as presented in Fig. 7 (g). At 700 kΩ, the load resistance, the highest power of 53.08 µW/cm^2, is reached, indicating that this is the CGC-TENG's optimum internal resistance. Fig. 7 (h) depicts the effect of sponge size and force applied on voltage generation using CGC-TENG. It's observed that the sponge size of 2 cm and force applied at 15 N generated the highest voltage. When applied force increases in the TENG device, voltage output increases by enhancing the contact area and allowing good interexchange charges. The larger device separation between materials after recontacting a higher charge imbalance results in a higher electrical output. Both factors improve TENG device charge retention and transfer [59, 60].

Low-power electronic devices can only function properly when supplied with a constant DC signal. As a consequence of this, the AC signal that is produced by TENGs cannot be utilized in order to activate these devices directly. TENGs, in conjunction with energy storage systems, must be used to supply low-power electronic devices with continuous DC power. As a result, the AC voltage of the output CGC-TENG was rectified using a rectifier and utilized to charge a capacitor. Fig. 8 (a) displays the circuit block diagram of the capacitor charging setup. A digital multimeter is used to monitor the capacitor charging process via CGC-TENG. The charging curves of several capacitors, 15 mF to 45 mF, for 200 seconds using CGC-TENG at 7 Hz frequency are shown in Fig. 7 (f), the highest frequency achieved with mechanical tapping. These capacitors had enough energy to power small electronic devices.

3.5 CGC-TENG Real-Time Device-level Applications

CGC-TENG's primary objective is to be used in real-time device-level applications. It's demonstrated the capability of our CGC-TENG to collect energy by powering several low-power consumption electrical devices. To begin, we ignited commercial blue LEDs with our CGC-TENG. Fig. 8 (b) shows twenty-three LEDs arranged in the alphabetical representations depicting "CUI" and linked in series using CGC-TENG. The power supplied by CGC-TENG using manual tapping was subsequently used to power such LEDs directly. When the room lights are turned off, the LEDs illumination becomes more visible, as shown in Fig. 8 (c). This example shows how easily our CGC-TENG can power LEDs (7.1 mW).

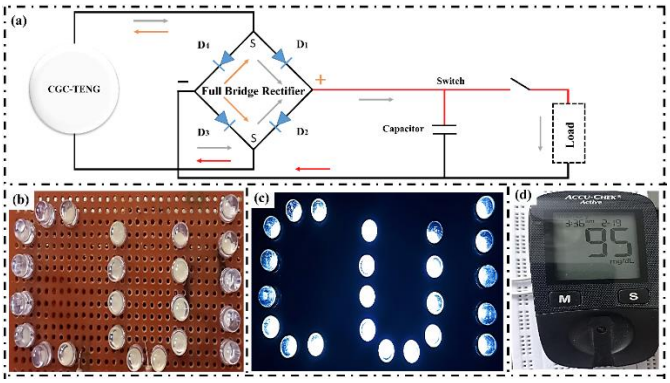

Fig. 8. Demonstration of CGC-TENG-based less energy use portable electronics devices: (a) A circuit schematic of a system incorporating a CGC-TENG (δ), a capacitor, and a rectifier for portable power gadgets. (b and c) show twenty-three commercial LEDs (left) linked in a series and controlled precisely by CGC-TENG (δ). Lights turn ON and OFF to demonstrate the flashing of the LEDs. (right-left). (d) Photogruyj7aphs of the digital electronic glucose monitoring, driven by CGC-TENG (δ).

According to the circuit block diagram illustrated in Fig. 8 (a), to provide power to portable electronic devices, a capacitor within the CGC-TENG. The system is divided into two major blocks: the CGC-TENG merged block linked via a series connected to a full bridge rectifier and a capacitor with the circuit. For changing A.C signals to D.C, use four diodes as a common bridge rectifier, and in order to provide continuous power to electronic devices for an extended period, use a capacitor as an energy storing device. The rectifier's positive terminal is linked to the capacitor's

positive terminal. In contrast, the negative terminal is linked to the capacitor's negative terminal, and the switch is linked to the capacitor's positive terminal and the portable electronic device. A switch turns ON to power the gadgets once the capacitor has been charged to the required level. A digital glucose monitoring device was chosen from among the portable electronic devices to be controlled by our CGC-TENG. Charging a 66 F capacitor for 60 seconds using a CGC-TENG device to power the glucose device. Fig. 8(d) shows that this portable glucose monitoring device worked for 10 seconds using a 66 F capacitor. The efficient operation of these gadgets suggests that our CGC-TENG derived from waste could be utilized to power the low-power consumption electronic gadgets.

4. Conclusion

The current work discusses the synthesis, low-cost fabrication of printable EHD electrospray, and operation of CDs/graphite nanocomposite-based CGC-TENG in harvesting electrical energy (voltage and current) from diverse mechanical energy (force applied) sources for operating low energy consumption portable electronic devices. The suggested CGC-TENG was created in an environmentally responsible manner by recycling wastes and carbon-based nanoparticles that boost TENG's performance. Furthermore, the suggested fabrication approach is easy, quick, and simple to use in our normal environment. The prototype CGC-TENGs performed admirably, the highest electrical output was obtained using CGC-TENG (δ) with an open-circuit voltage of 171.30 V, a short circuit current of 111.39 μA, and a maximum output power density of 53.08 $\mu W/cm^2$ achieved. When Carbon Dots (CDs) were employed, the TENG device produced a high voltage of 127.31 V and a current of 107.12 μA; without CDs, it produced a low voltage of 95.23 V and a current of 104.12 μA. CDs in the graphite matrix boost CGC-TENG's electrical output. The electrical output performance of CGC-TENG with CDs is much higher than without CDs. It's demonstrated the CGC-TENG (δ) can power an electronic glucose monitoring device and twenty-three blue LEDs, proving its usefulness in energy-consumption portable electronic devices. The proposed CGC-TENGs are entirely made of household recyclable materials, which is consistent with the globular low-cost concept because not only are the triboelectric active layers but also other materials can be recycled and recovered from electronic trash. The paper-based triboelectric layer is eco-friendly, and also another triboelectric layer made of plastic is recovered from unwanted plastic bottles; the proposed CGC-TENG decreases environmental contamination and promotes sustainable development.

5. Acknowledgment

The Higher Education Commission of Pakistan (HEC) funded this research under National Research Fund project # 7278/Federal/NRPU/R&D/HEC/2017. The findings presented here reflect the research and are solely the authors' responsibility.

6. Abbreviations

A	Current
A.C	Alternative Current
Al	Aluminum
CDs	Carbon Dots
CGC	Carbon Dots Graphite Nano Composite
Cu	Copper
CUI	COMSATS University Islamabad
D.C	Direct Current
EHD	Electro Hydrodynamics
E-Waste	Electronic Waste
HEC	Higher Education Commissions
K.W.	Kilo Watt
TENGs	Tribo Electro Nano Generators
V	Voltage

7. References

[1] B. Chander, S. Pal, D. De, and R. Buyya, "Artificial intelligence-based internet of things for industry 5.0," Artificial intelligence-based internet of things systems, pp. 3-45, 2022.

[2] B. G. Mohammed and D. S. Hasan, "Smart healthcare monitoring system using IoT," International Journal of Interactive Mobile Technologies, vol. 17, no. 01, pp. 141-152, 2023.

[3] N. Srivastava and P. Pandey, "Internet of things (IoT): Applications, trends, issues and challenges," Materials Today: Proceedings, vol. 69, pp. 587-591, 2022.

[4] D. S. Renné, "The opportunities and challenges for 100% renewable energy," 2022, pp. 495-503: Springer.

[5] Y. M. Li, Y. Wang, M. J. Chen, T. Y. Huang, F. H. Yang, and Z. J. Wang, "Current status and technological progress in lead recovery from electronic waste," International Journal of Environmental Science and Technology, vol. 20, no. 1, pp. 1037-1052, 2023.

[6] R. Rajesh, D. Kanakadhurga, and N. Prabaharan, "Electronic waste: A critical assessment on the unimaginable growing pollutant, legislations and environmental impacts," Environmental Challenges, vol. 7, p. 100507, 2022.

[7] M. V. Ramesh, M. Paramasivan, P. Akshay, and T. Jarin, "A review on electric and electronic waste material management in 21st century," Materials Today: Proceedings, 2023.

[8] P. E. Karthik, H. Rajan, V. R. Jothi, B.-I. Sang, and S. C. Yi, "Electronic wastes: A near inexhaustible and an unimaginably wealthy resource for water splitting electrocatalysts," Journal of Hazardous Materials, vol. 421, p. 126687, 2022.

[9] D. Sakhuja, H. Ghai, R. K. Bhatia, and A. K. Bhatt, "Management of e-waste: technological challenges and opportunities," Handbook of Solid Waste Management: Sustainability through Circular Economy, pp. 1523-1557, 2022.

[10] R. Golmohammadzadeh, F. Faraji, B. Jong, C. Pozo-Gonzalo, and P. C. Banerjee, "Current challenges and future opportunities toward recycling of spent lithium-ion batteries," Renewable and Sustainable Energy Reviews, vol. 159, p. 112202, 2022.

[11] M. Iturrondobeitia, O. Akizu-Gardoki, O. Amondarain, R. Minguez, and E. Lizundia, "Environmental impacts of aqueous zinc ion batteries based on life cycle assessment," Advanced Sustainable Systems, vol. 6, no. 1, p. 2100308, 2022.

[12] P. Li, X. Xia, and J. Guo, "A review of the life cycle carbon footprint of electric vehicle batteries," Separation and Purification Technology, vol. 296, p. 121389, 2022.

[13] J. Quan, S. Zhao, D. Song, T. Wang, W. He, and G. Li, "Comparative life cycle assessment of LFP and NCM batteries including the secondary use and different recycling technologies," Science of The Total Environment, vol. 819, p. 153105, 2022.

[14] M. Salado and E. Lizundia, "Advances, challenges, and environmental impacts in metal–air battery electrolytes," Materials Today Energy, vol. 28, p. 101064, 2022.

[15] X. Wang, G. Gaustad, C. W. Babbitt, C. Bailey, M. J. Ganter, and B. J. Landi, "Economic and environmental characterization of an evolving Li-ion battery waste stream," Journal of environmental management, vol. 135, pp. 126-134, 2014.

[16] F. Wu et al., "Environmental hotspots and greenhouse gas reduction potential for different lithium-ion battery recovery strategies," Journal of Cleaner Production, vol. 339, p. 130697, 2022.

[17] N. Ferronato and V. Torretta, "Waste mismanagement in developing countries: A review of global issues," International journal of environmental research and public health, vol. 16, no. 6, p. 1060, 2019.

[18] M. G. Kibria, N. I. Masuk, R. Safayet, H. Q. Nguyen, and M. Mourshed, "Plastic waste: challenges and opportunities to mitigate pollution and effective management," International Journal of Environmental Research, vol. 17, no. 1, p. 20, 2023.

[19] C. Polprasert, T. Yeemin, M. Sutthacheep, T. Pussayanavin, K. Jinda, and S. Kamngam, "Marine ecosystems and emerging plastic pollution," MARINE PLASTICS ABATEMENT, p. 85, 2023.

[20] B. Sainte-Rose, Y. Pham, and W. Pavalko, "Persistency and surface convergence evidenced by two maker buoys in the great pacific garbage patch," Journal of Marine Science and Engineering, vol. 11, no. 1, p. 68, 2023.

[21] X. Liang, W. Dang, G. Yang, and Y. Zhang, "Environmental feasibility evaluation of cement co-production using classified domestic waste as alternative raw material and fuel: A life cycle perspective," Journal of Environmental Management, vol. 326, p. 116726, 2023.

[22] B. Nyberg, P. T. Harris, I. Kane, and T. Maes, "Leaving a plastic legacy: Current and future scenarios for mismanaged plastic waste in rivers," Science of the Total Environment, vol. 869, p. 161821, 2023.

[23] I. C. M. Candido et al., "PVA-silk fibroin bio-based triboelectric nanogenerator," Nano Energy, vol. 105, p. 108035, 2023.

[24] X. Chen, N. Kroell, M. Althaus, T. Pretz, R. Pomberger, and K. Greiff, "Enabling mechanical recycling of plastic bottles with shrink sleeves through near-infrared spectroscopy and machine learning algorithms," Resources, Conservation and Recycling, vol. 188, p. 106719, 2023.

[25] J. Luo, W. Gao, and Z. L. Wang, "The triboelectric nanogenerator as an innovative technology toward intelligent sports," Advanced materials, vol. 33, no. 17, p. 2004178, 2021.

[26] Y. Peng et al., "A review of recent development of wearable triboelectric nanogenerators aiming at human clothing for energy conversion," Polymers, vol. 15, no. 3, p. 508, 2023.

[27] C. Piguet, Low-power electronics design. CRC press, 2018.

[28] M. Sahu, S. Hajra, K. Lee, P. L. Deepti, K. Mistewicz, and H. J. Kim, "Piezoelectric nanogenerator based on lead-free flexible PVDF-barium titanate composite films for driving low power electronics," Crystals, vol. 11, no. 2, p. 85, 2021.

[29] S. An et al., "Deep learning enabled neck motion detection using a triboelectric nanogenerator," ACS nano, vol. 16, no. 6, pp. 9359-9367, 2022.

[30] C. Lin, H. Zhao, H. Huang, X. Ma, and S. Cao, "PEO/cellulose composite paper based triboelectric nanogenerator and its application in human-health detection," International Journal of Biological Macromolecules, vol. 228, pp. 251-260, 2023.

[31] J. Park, I. Kim, J. Yun, and D. Kim, "Liquid-metal embedded sponge-typed triboelectric nanogenerator for omnidirectionally detectable self-powered motion sensor," Nano Energy, vol. 89, p. 106442, 2021.

[32] S. M. A. Z. Shawon et al., "Piezo-tribo dual effect hybrid nanogenerators for health monitoring," Nano Energy, vol. 82, p. 105691, 2021.

[33] K. V. Vijoy, H. John, and K. J. Saji, "Self-powered ultra-sensitive millijoule impact sensor using room temperature cured PDMS based triboelectric nanogenerator," Microelectronic Engineering, vol. 251, p. 111664, 2022.

[34] X. Feng, Q. Li, and K. Wang, "Waste plastic triboelectric nanogenerators using recycled plastic bags for power generation," ACS Applied Materials & Interfaces, vol. 13, no. 1, pp. 400-410, 2020.

[35] M. A. Jalili, Z. Khosroshahi, N. R. Kheirabadi, F. Karimzadeh, and M. H. Enayati, "Green triboelectric nanogenerator based on waste polymers for electrophoretic deposition of titania nanoparticles," Nano Energy, vol. 90, p. 106581, 2021.

[36] G. Prasad, S. A. Graham, J. S. Yu, H. Kim, and D.-W. Lee, "Investigated a PLL surface-modified Nylon 11 electrospun as a highly tribo-positive frictional layer to enhance output performance of triboelectric nanogenerators and self-powered wearable sensors," Nano Energy, vol. 108, p. 108178, 2023.

[37] M. Wu et al., "A hybrid triboelectric nanogenerator for enhancing corrosion prevention of metal in marine environment," npj Materials Degradation, vol. 6, no. 1, p. 73, 2022.

[38] A. Ravikumar et al., "Piezoelectric nanogenerator induced work function on a metal phenolic coordination framework from copper oxide nanospheres for efficient biomechanical energy harvesting and physiological monitoring," Journal of Materials Chemistry C, vol. 10, no. 43, pp. 16492-16505, 2022.

[39] L. Sarkar, M. V. Sushma, B. P. Yalagala, A. K. Rengan, S. G. Singh, and S. R. K. Vanjari, "ZnO nanoparticles embedded silk fibroin—a piezoelectric composite for nanogenerator applications," Nanotechnology, vol. 33, no. 26, p. 265403, 2022.

[40] S. Veeralingam and S. Badhulika, "Lead-free transparent flexible piezoelectric nanogenerator for self-powered wearable electronic sensors and energy harvesting through rainwater," ACS Applied Energy Materials, vol. 5, no. 10, pp. 12884-12896, 2022.

[41] C. Yoon et al., "Synergistic contribution of flexoelectricity and piezoelectricity towards a stretchable robust nanogenerator for wearable electronics," Nano Energy, vol. 91, p. 106691, 2022.

[42] X. Li et al., "Metal ions-doped carbon dots: Synthesis, properties, and applications,"

Chemical Engineering Journal, vol. 430, p. 133101, 2022.

[43] S. Sengupta, S. Pal, A. Pal, S. Maity, K. Sarkar, and M. Das, "A review on synthesis, toxicity profile and biomedical applications of graphene quantum dots," Inorganica Chimica Acta, p. 121677, 2023.

[44] B. Wang, H. Cai, G. I. N. Waterhouse, X. Qu, B. Yang, and S. Lu, "Carbon dots in bioimaging, biosensing and therapeutics: a comprehensive review," Small science, vol. 2, no. 6, p. 2200012, 2022.

[45] B. Wang and S. Lu, "The light of carbon dots: From mechanism to applications," Matter, vol. 5, no. 1, pp. 110-149, 2022.

[46] D. Sarkar et al., "High β-crystallinity comprising nitrogenous carbon dot/PVDF nanocomposite decorated self-powered and flexible piezoelectric nanogenerator for harvesting human movement mediated energy and sensing weights," Ceramics International, vol. 49, no. 3, pp. 5466-5478, 2023.

[47] Y. Zhai et al., "Carbon dots as new building blocks for electrochemical energy storage and electrocatalysis," Advanced Energy Materials, vol. 12, no. 6, p. 2103426, 2022.

[48] Z. Esa, M. Abid, J. H. Zaini, B. Aissa, and M. M. Nauman, "Advancements and applications of electrohydrodynamic printing in modern microelectronic devices: a comprehensive review," Applied Physics A, vol. 128, no. 9, p. 780, 2022.

[49] Y. Guan, S. Wu, M. Wang, Y. Tian, W. Lai, and Y. Huang, "Numerical analysis of electrohydrodynamic jet printing under constant and step change of electric voltages," Physics of Fluids, vol. 34, no. 6, 2022.

[50] N. Mkhize and H. Bhaskaran, "Electrohydrodynamic jet printing: Introductory concepts and considerations," Small Science, vol. 2, no. 2, p. 2100073, 2022.

[51] Y. Bai, H. Feng, and Z. Li, "Theory and applications of high-voltage triboelectric nanogenerators," Cell Reports Physical Science, vol. 3, no. 11, 2022.

[52] K. Muldoon, Y. Song, Z. Ahmad, X. Chen, and M.-W. Chang, "High precision 3d printing for micro to nano scale biomedical and electronic devices," Micromachines, vol. 13, no. 4, p. 642, 2022.

[53] Y. Dong et al., "Carbon-based dots co-doped with nitrogen and sulfur for high quantum yield and excitation-independent emission," Angewandte Chemie, vol. 125, no. 30, pp. 7954-7958, 2013.

[54] Z. Li et al., "Highly luminescent nitrogen-doped carbon quantum dots as effective fluorescent probes for mercuric and iodide ions," Journal of Materials Chemistry C, vol. 3, no. 9, pp. 1922-1928, 2015.

[55] N. Das et al., "Piezoelectric activity assessment of size-dependent naturally acquired mud volcano clay nanoparticles assisted highly pressure sensitive nanogenerator for green mechanical energy harvesting and body motion sensing," Nano Energy, vol. 102, p. 107628, 2022.

[56] J. Luo and Z. L. Wang, "Recent progress of triboelectric nanogenerators: From fundamental theory to practical applications," EcoMat, vol. 2, no. 4, p. e12059, 2020.

[57] S. Niu and Z. L. Wang, "Theoretical systems of triboelectric nanogenerators," Nano Energy, vol. 14, pp. 161-192, 2015.

[58] J. Shao, M. Willatzen, and Z. L. Wang, "Theoretical modeling of triboelectric nanogenerators," Journal of Applied Physics, vol. 128, no. 11, 2020.

[59] J. Wang et al., "Enhancing output performance of triboelectric nanogenerator via charge clamping," Advanced Energy Materials, vol. 11, no. 31, p. 2101356, 2021.

[60] Z. Wang et al., "Two voltages in contact-separation triboelectric nanogenerator: from asymmetry to symmetry for maximum output," Nano Energy, vol. 69, p. 104452, 2020.

